Geodesic chaos around quadrupolar deformed centers of attraction

Eduardo Guéron* and Patricio S. Letelier†
Departamento de Matemática Aplicada, Instituto de Matemática, Estatística e Computação Científica, Universidade Estadual de Campinas, 13083-970 Campinas, SP, Brazil
(Received 18 April 2002; published 16 October 2002)

The exact solution to the Einstein equations that represent a static axially symmetric source deformed by an internal quadrupole is considered. The Poincaré section method is used to study numerically the geodesic motion of test particles, for prolate quadrupole deformations, we find chaotic motions contrary to the oblate case where only regular motion is found. We also consider the metric that represents a rotating black hole deformed by a quadrupole term. This metric is obtained as a two-soliton solution in the context of Belinsky-Zakharov inverse scattering method. The stability of geodesics depends strongly on the relative direction of the spin of the center of attraction and the angular momentum of the test particle.

DOI: 10.1103/PhysRevE.66.046611 PACS number(s): 95.10.Fh, 05.45.−a, 04.20.Jb

INTRODUCTION

After the visionary work of the Poincaré [1] and the KAM (Kolmogorov, Arnold, and Moser [2]) theories, it became well established that nonintegrability, and hence chaos, is a general rather than exceptional manifestation in the context of dynamical systems, see for instance, Ref. [3]. Given this ubiquitous fact, an important issue in astronomical modeling is the study in which extent in phase space chaoticity rises in models that are relevant to describe real systems and what are its consequences.

The adequate description of the gravitation field of an astrophysical object has been an important subject in both relativistic and Newtonian gravity since their origin. The particular case of the gravity associated to an axially symmetric body has played a central role in this discussion. Recently, Merrit [4] found, from detailed modeling of triaxial galaxies, that most of the galaxies must be nearly axisymmetric, either prolate or oblate. In Newtonian theory the gravitational potential of an axially symmetric body can be always represented by its usual expansion in terms of the Legendre polynomials (zonal harmonics). The underlying theory in this case is the usual Newtonian gravitation that, for large masses and velocities, is known to be less appropriate than the Einstein general relativity. In the latter case the Newtonian potential is replaced by the space-time metric and Newton motion equations by geodesics. In general relativity, we have that the solution of the vacuum Einstein equations associated to a static axially symmetric body has a simple form with only two metric functions [5], and one of them admits an expansion in zonal harmonics. For rotating axially symmetric bodies we have a metric with three functions and two of them obey a sigma-model type of partial differential equations for which there are known methods of solution [6].

The change of the particle motion equation and gravitational theory can produce dramatic effects, for instance, test particles moving in the presence of systems of masses, which are integrable in Newtonian theory are chaotic in general relativity; examples are the fixed two-body problem [7,8], and particles moving in a monopolar center of attraction surrounded by a dipolar halo [9]. Also gravitational waves, a nonexisting phenomenon in the Newtonian realm, can produce irregular motion of test particles orbiting around a static black hole [10,11]. Another distinctive feature of general relativity is the dragging of inertial frames due to mass rotation. This fact is observed, for instance, in the impressive differences of the geodesic motion in Schwarzschild and Kerr geometries [12].

Along this paper we shall study the geodesic equations for particles evolving in the space time associated to a center of attraction with a quadrupolar deformation. The solution of the Einstein equations representing this center of attraction—in the static case—can be found in Ref. [13], wherein the rather misleading terminology ''distorted black hole'' was used to refer to such an object. Examples of static centers of attractions with multipolar deformations are:

(a) A true static black hole (or a dense object) surrounded by a distribution of matter like a ring or a small disk formed by counter-rotating matter, i.e., built by approximately the same number of particles moving clockwise as counterclockwise. Even though this interpretation can be seen as a device to have a static stable configuration, there is observational evidence of disks made of streams of rotating and counter-rotating matter [14].

(b) An axially symmetric static dense object with either polar deformations or polar jets. In the case (a) we have oblate deformations. Also the polar deformations of the Sun and the inner planets in the solar system are oblate. We have prolate deformations in stars with jets and in some galaxy clusters [15]. In the precedent cases, by adding rotation to the central black hole and removing the counter-rotating hypothesis we can have stationary centers of attraction with multipolar deformations. We recall that accordingly to the nonhair black hole theorems, a noncharged black hole is completely characterized by its angular momentum and mass, therefore any multipolar deformation for a true black hole must be interpreted as structures located outside the event horizon, which break the spherical symmetry of the system [16].

Geodesic motions for axially symmetric space times rep-

*Email address: gueron@ime.unicamp.br
†Email address: letelier@ime.unicamp.br

resenting core-halo system were studied in Ref. [17] for bounded motion and in Ref. [18] for unbounded motions. The case of a slowly rotating center of attraction with a dipolar halo was considered in Ref. [19]. The geodesic chaos for a disk with a central center of attraction was considered in [20]. A core-halo system with Newman-Unti-Tamburino charge was also considered [21]. Newtonian [22] and pseudo-Newtonian [23] counterparts of some of these systems were also studied. In a recent paper—within the Newtonian realm—we studied chaotic motions of test particles orbiting around a deformed body modeled by a monopolar and an internal quadrupolar term [24].

In this paper, we dwell in the study of geodesic chaos, but now related to *internal* quadrupole deformations of the attraction center. Note that halos are external multipolar contributions, their strength increases with the distance, contrary to the internal ones that decrease with the distance. The quadrupolar contribution usually represents the major deviation to the spherical symmetry. Thus, as a good first approximation, it can model most of the deformed sources.

We shall analyze only bounded motions for specific choices of energy and angular momentum and certain values of quadrupolar strength that we believe will cover all the different typical situations. Due to the symmetry of the problem, one can reduce the geodesic motion to a dynamical system with two degrees of freedom. For such cases, the Poincaré section method is the most appropriated tool to study the general behavior of the geodesics.

In the first one, Sec. I, the exact solution to the Einstein equations, which represents a static axially symmetric source deformed by an internal quadrupole, is considered. The Poincaré section method is used to study numerically the geodesic motion of test particles orbiting around a deformed source, for prolate quadrupolar deformations we find chaotic motion contrary to the oblate case where only regular motion is found.

In the second one, Sec. II, the rotation of the attraction center is considered. We first study the metric that represents a rotating black hole deformed by a quadrupolar term. This metric is obtained as a two-soliton solution in the context of Belinsky-Zakharov inverse scattering method [25] that generates new solutions from a known one (seed solution). As in the preceding section, geodesics are numerically studied using surfaces of section. The consideration of different cases leads us to conclude that the black hole rotation considerably alters the stability of the system. We obtain that the stability depends strongly on the relative direction of the spin of the center of attraction and the angular momentum of the test particle. We also find that the rotation does not alter the regular character of geodesic motions in the oblate case, i.e., the orbits in this case remain regular. Finally, we discuss and summarize the obtained results. We also present and discuss some Poincaré sections for test particles moving in the gravitational field of a monopole with large rotation surrounded by a dipolar halo.

I. SCHWARZSCHILD SOLUTION WITH QUADRUPOLE DEFORMATIONS

The metric of the space time related to the gravitational field of a static axially symmetric source is the one associated with the Weyl line element,

$$ds^2=e^{2\psi}dt^2-e^{2(\gamma-\psi)}(dz^2+dr^2)-r^2e^{-2\psi}d\varphi^2, \quad (1)$$

where ϕ and γ are functions of r and z only. The range of the coordinates r,z,φ are the usual ones for cylindrical coordinates. It is more convenient to use prolate spheroidal coordinates u and v, which are related to the Weyl coordinates by

$$r^2=m^2(u^2-1)(1-v^2), \quad (2)$$

$$z=muv,$$

where m is a constant that reports to the mass of the center of attraction. The coordinate v takes values in the interval $[-1,1]$ (it is essentially a cosine) and u runs from 1 to infinity (it is essentially a radial coordinate). We shall use units such that $c=G=1$. With no loss of generality we shall also choose $m=1$. In this new system of coordinates, the metric (1) takes the form,

$$ds^2=e^{2\psi(u,v)}dt^2-e^{-2\psi(u,v)}(u^2-1)(1-v^2)d\phi^2 - e^{2(\gamma(u,v)-\psi(u,v))}(u^2-v^2)\left(\frac{du^2}{u^2-1}+\frac{dv^2}{1-v^2}\right). \quad (3)$$

For this line element, the vacuum Einstein equations reduces to

$$[(u^2-1)\psi_{,u}]_{,u}+[(1-v^2)\psi_{,v}]_{,u}=0, \quad (4)$$

$$\gamma_{,u}=\frac{(u\psi_{,u}-2v\psi_{,v})(u^2-1)(1-v^2)\psi_{,u}-u(1-v^2)^2\psi_{,v}{}^2}{(u^2-v^2)},$$

$$\gamma_{,v}=\frac{(2u\psi_{,u}-v\psi_{,v})(u^2-1)(1-v^2)\psi_{,v}+v(u^2-1)^2\psi_{,u}{}^2}{(u^2-v^2)}. \quad (5)$$

Equation (4) is the usual Laplace equation in prolate coordinates for the metric potential ψ, and Eqs. (5) yield the function γ as a quadrature. The integrability of γ ($\gamma_{,uv}=\gamma_{,vu}$) is guaranteed by Eq. (4). The potential ψ for the Schwarzschild solution in prolate coordinates is [5]

$$\psi_S=\frac{1}{2}\ln\frac{1-u}{1+u}. \quad (6)$$

In this paper we shall consider the solution

$$\psi=\frac{1}{2}\ln\frac{1-u}{1+u}+k_2P_2(v)Q_2(u), \quad (7)$$

where P_2 and Q_2 are the second Legendre polynomial and function, respectively,

$$P_2(x)=(3x^2-1)/2,$$

$$Q_2(x)=\{P_2(x)\ln[(x+1)/(x-1)]-3x\}/2, \tag{8}$$

and k_2 is a constant that is positive (negative) for oblate (prolate) deformations. Note that the Newtonian limit of the potential (7) is $\phi=-m/R+(2m^3k_2/15)P_2(\cos\vartheta)R^{-3}$ (we use the definition of Newtonian limit of Ref. [27]).

From Eq. (5), we find the other metric function,

$$\begin{aligned}\gamma=\{&4[2((7k_2^2-20k_2+4)\ln(u-1)+(k_2+2)^2\ln(u+1)\\&-4\ln(u^2-v^2)(k_2-1)^2)-3((27u^2v^2-30u^2\\&-21v^2+26)k_2-8)\ln((u+1)/(u-1))k_2uv^2\\&+3((27u^2v^4-30u^2v^2+3u^2-12v^4+16v^2)k_2\\&-16v^2)k_2]-3[4((3u^2-3u-2)k_2+8)\\&-3(9u^2v^2-u^2-v^2+1)(u-1)(v^2-1)\\&\times\ln((u+1)/(u-1))k_2](u+1)\\&\times\ln((u+1)/(u-1))k_2\}/64.\end{aligned} \tag{9}$$

The exact solution to Einstein equations given by Eqs. (7)–(9) was first studied by Erez and Rosen [28]. The general case (Schwarzschild with the whole series of multipoles) was considered by Quevedo [29], and a simple interpretation in terms of bars was presented by Letelier [30]. This solution is interpreted as a ''distorted'' black hole in Ref. [13]. The study of the associated Newtonian multipoles, as well as the relativistic multipoles for this solution and other multipolar expansions can be found in Ref. [31]. The geodesic equations for the metric (3) take the form

$$\begin{aligned}\frac{d^2u}{d\tau^2}=&\frac{u^2-1}{2e^{2(\gamma-\psi)}(u^2-v^2)}\\&\times\{\partial_ue^{2\psi}+\partial_u[(u^2-1)(1-v^2)e^{-2\psi}]\}\\&-\dot u^2\left([\partial_u(\gamma-\psi)]+\frac{(v^2-1)u}{(u^2-v^2)(u^2-1)}\right)\\&-2\dot u\dot v\left([\partial_v(\gamma-\psi)]-\frac{v}{(u^2-v^2)}\right)\\&-\dot v^2\left(\frac{(u^2-1)[\partial_u(\gamma-\psi)]}{(v^2-1)}+\frac{(u^2-1)u}{(u^2-v^2)(v^2-1)}\right),\end{aligned} \tag{10}$$

$$\begin{aligned}\frac{d^2v}{d\tau^2}=&\frac{1-v^2}{2e^{2(\gamma-\psi)}(u^2-v^2)}\\&\times\{\partial_ve^{2\psi}+\partial_v[(u^2-1)(1-v^2)e^{-2\psi}]\}\\&-\dot v^2\left([\partial_v(\gamma-\psi)]-\frac{(u^2-1)v}{(u^2-v^2)(v^2-1)}\right)\\&-2\dot u\dot v\left([\partial_u(\gamma-\psi)]+\frac{u}{(u^2-v^2)}\right)\\&-\dot u^2\left(\frac{(v^2-1)[\partial_v(\gamma-\psi)]}{(u^2-1)}-\frac{(v^2-1)v}{(u^2-v^2)(u^2-1)}\right),\end{aligned} \tag{11}$$

$$E=e^{2\psi(u,v)}\dot t,\quad L=e^{-2\psi(u,v)}(u^2-1)(1-v^2)\dot\varphi, \tag{12}$$

where $\tau=s/c=s$ and the overdots indicate derivative with respect τ. E and L are constants of integrations related to the test particle energy and the angular momentum, respectively. The metric (3) gives a third constant of motion,

$$\begin{aligned}1=&e^{2\psi(u,v)}\dot t^2-e^{-2\psi(u,v)}(u^2-1)(1-v^2)\dot\varphi^2\\&-e^{2(\gamma(u,v)-\psi(u,v))}(u^2-v^2)\left(\frac{\dot u^2}{u^2-1}+\frac{\dot v^2}{1-v^2}\right).\end{aligned} \tag{13}$$

The motion of the test particle is completely determined by the solution of the two second-order differential equations (10) and (11). They define a four-dimensional phase space, but the motion constants (13) and (12) tell us that the motion is effectively realized in a three-dimensional surface. Moreover, these constants allow us to define an effective potential-like function,

$$\begin{aligned}\Phi(u,v)=&\frac{e^{2(\psi(u,v)-v(u,v))}}{(u^2-v^2)}\left(e^{-2\psi(u,v)}E^2\right.\\&\left.-\frac{e^{2(\psi(u,v)-v(u,v))}}{(u^2-1)(1-v^2)}L^2-1\right).\end{aligned} \tag{14}$$

Thus the motion must be restricted to the region defined by the inequality $\Phi(u,v)\leqslant 0$.

Since the geodesic motion of the test particles is performed in a three-dimensional effective phase space, an adequate tool to study this motion is the Poincaré section

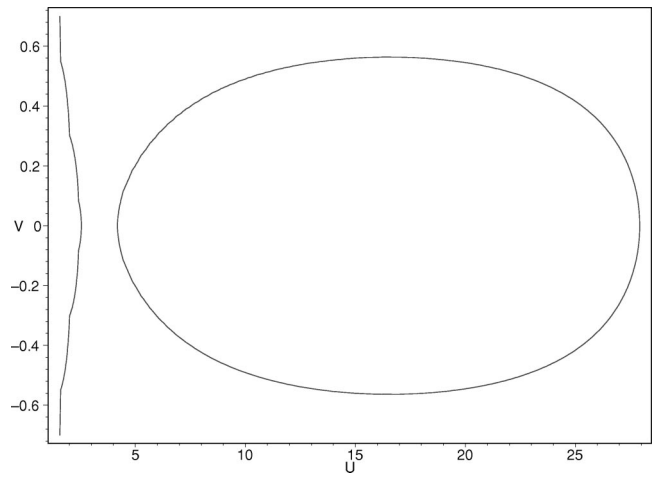

FIG. 1. Boundary contour for $L=3.8$, $E=0.973$, and $k_2=-1.0$. There is an escape zone and one region of bounded motion. u and v are dimensionless.

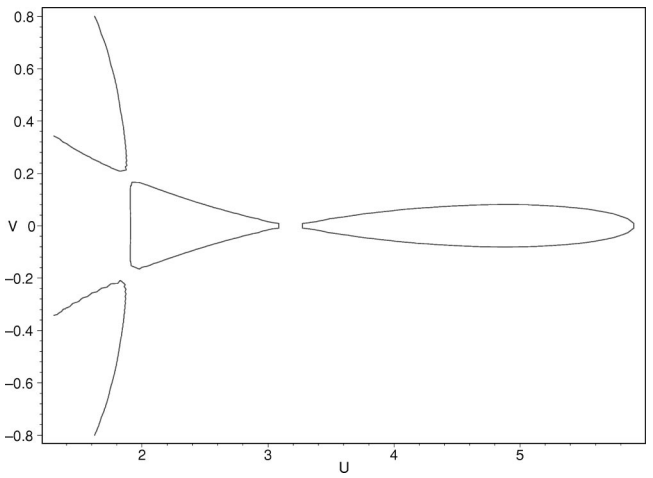

FIG. 3. Same values of the preceding figure, but now $k_2=-5.02$. There are two escape zones in the left-hand side of the picture and two closed zones of bounded motion.

method. As we mention before, the sign of the quadrupole parameter k_2 specifies whether the source is deformed in a prolate or in an oblate shape.

A. Prolate deformation

First we shall study the prolate case, $k_2<0$. From relation (14), we find the appropriated constants to have a confined motion. We have that only three combinations of the constants: E (energy), L (angular momentum), and k_2 (quadrupole strength) typify all the possibilities of confinement.

In Fig. 1 we present the curve $\Phi(u,v)=0$ for $L=3.8$, $E=0.9731$, and $k_2=-1$, this is the most common situation found for bounded internal prolate quadrupole solutions. There is only one smooth closed surface. The case $L=3.32$, $E=0.937$, and $k_2=-5.0$ is presented in Fig. 2, we still see only one closed surface, but now we have two regions linked by a narrow connection. Finally, in Fig. 3, we present the curve $\Phi(u,v)=0$ for $L=3.32$, $E=0.937$, and $k_2=-5.02$, we have two disconnected bounded regions. This last situation is quite different in the Newtonian limit wherein the bounded surface is separated in two regions: one above and other below the equatorial plane as shown in Fig. 4(d). In other words, we can say that in the general relativistic case the closed surfaces are two concentric rings, while in the Newtonian theory one is the reflection of the other under the plane $z=0$.

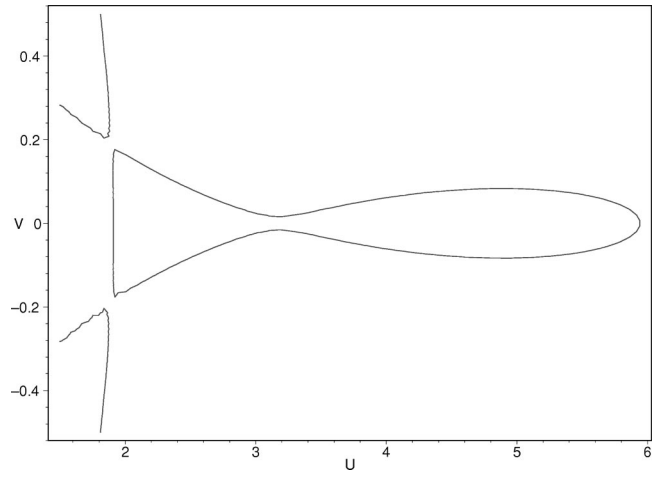

FIG. 2. Boundary contour for $L=3.32$, $E=0.937$, and $k_2=-5.0$. There are two escape zones in the left-hand side of the picture, which correspond to small values of u, and a closed zone of bounded motion which is almost divided into two.

The behavior of orbits using Poincaré surface sections for each one of the three sets of constants indicated above is presented in Figs. 5–7. In Fig. 5 we show that the motion in the bounded region of Fig. 1 is regular as in the case of a pure Schwarzschild black hole [17]. In Fig. 6 we show the Poincaré section for orbits restricted to the closed surface

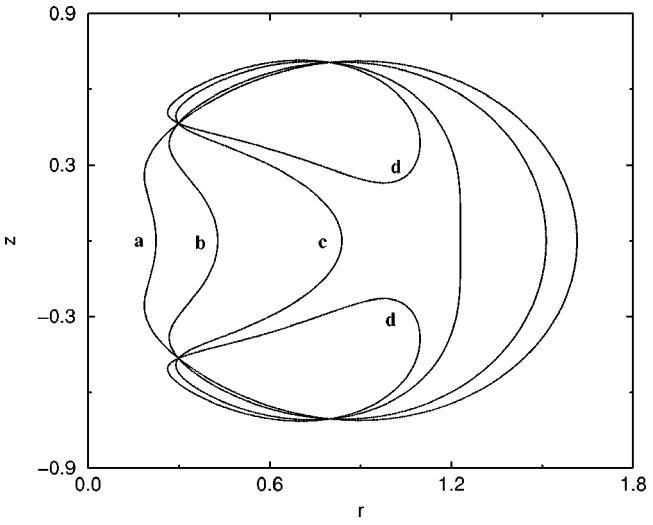

FIG. 4. A sequence of bounded regions in the Newtonian prolate quadrupole plus monopole solution. The lines d represent two closed surfaces separated by the plane $z=0$. The coordinates r and z are measured in geometric units, and the mass of the center of attraction is assigned the value of 1.

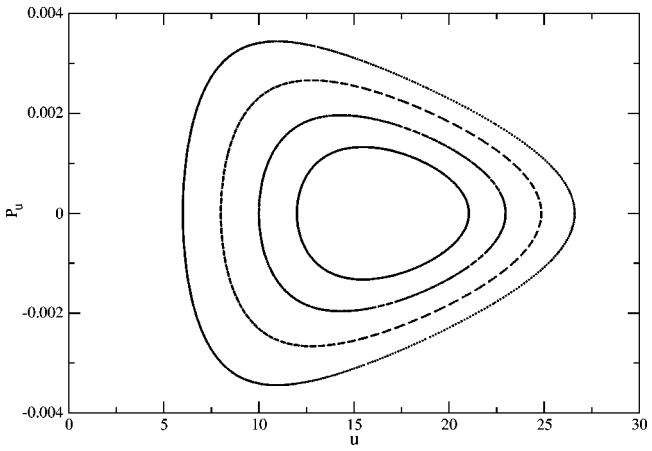

FIG. 5. Poincaré section for the values defined in Fig. 1. We have regular motion. $P_u \equiv du/d\tau$, τ is measured in geometric units with the unit of mass taken as in the preceding figure.

presented in Fig. 2. It is interesting to observe that we have a region of irregular motion on the right and a region of regular motion surrounded by a layer of chaos on the left. In Fig. 7 we present a Poincaré section for the two bounded regions of Fig. 3. In the bounded region of the left-hand side of the figure, we have a typical picture of chaotic motion, but orbits confined in the other bounded region present regular motion.

These results can be understood by studying the effective potential critical points. We recall that a pure black hole ($k_2=0$) with adequate values of the constants E and L has an effective potential with a single saddle point. When we add the prolate quadrupolar field $k_2<0$, we have a second saddle point for the value of the constants of Figs. 3 and 2. In the third case (Fig. 1) the second saddle point disappears, and we end up with the same dynamical behavior of the test particles as in the pure Schwarzschild black hole case. In the general relativistic example there can be two the saddle points on the plane $z=0$, while in the Newtonian analog we can have at most one in this plane [24].

B. Oblate deformation

For the case of oblate quadrupole deformation, i.e., $k_2>0$, we always find regions of bounded motion very similar

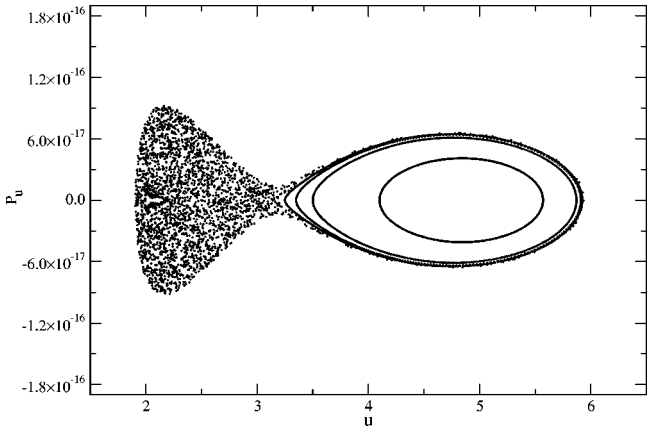

FIG. 6. Poincaré section for the values defined in Fig. 2. We see chaotic motion in the left-hand side of the figure and in a small external region on the right-hand side.

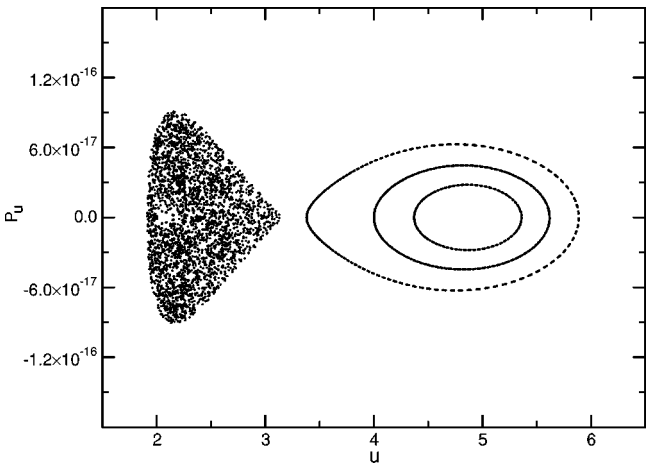

FIG. 7. Poincaré section for the values defined in Fig. 3. We see chaotic behavior in orbits confined in the first zone of bounded motions, but the motion in the second zone is regular.

to the one presented in Fig. 1. A configuration with two bounded regions, like the ones presented in Fig. 3, is not possible. The typical example is shown in Fig. 8, where $E=0.96$, $L=3.8$, and $k_2=5$. We see that there is just one bounded region, and the escape zone is not divided into two, like that in the prolate cases, i.e., the origin belongs to the escape region. This indicates the absence of a second saddle point, like that in the pure black hole situation. However, in the Newtonian limit, we can find one saddle point on the plane $z=0$.

The geodesics were studied using surface sections for many different values of E, L, and $k_2>0$. We find only regular motions. In Fig. 9 we present a typical Poincaré section for this case. The parameters are the ones of Fig. 8. We observe that, at least in our computer resolution, the tori of the total integrable situation are not destroyed.

II. KERR SOLUTION WITH QUADRUPOLE DEFORMATIONS

Since the Kerr solution represents a rotating black hole, the addition of an internal multipole term can be used to

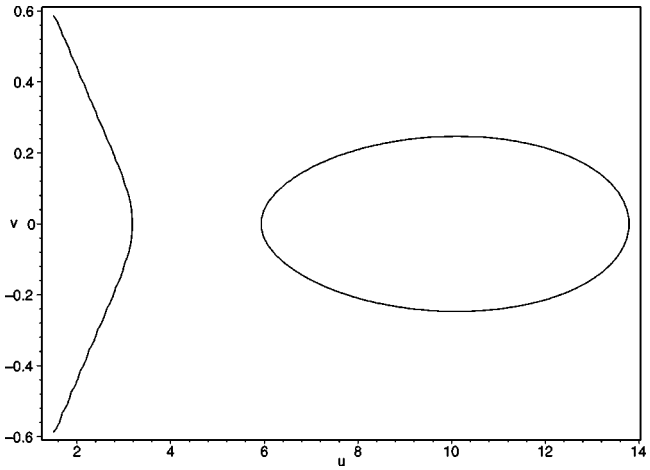

FIG. 8. Boundary contour for $L=3.8$ and $E=0.96$, but now $k_2=5.0$. We see one bounded region. The escape zone contains the origin.

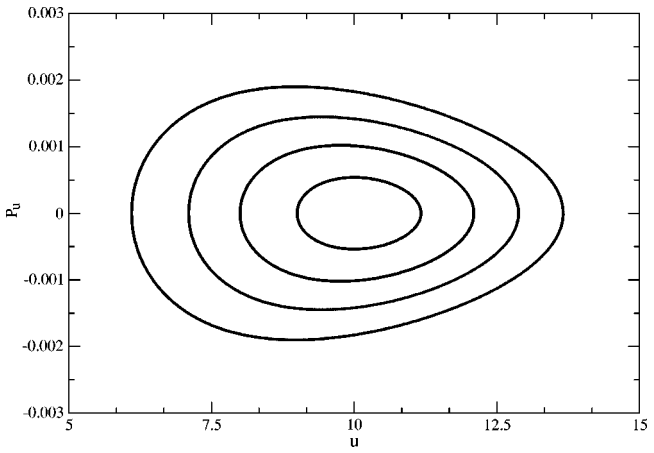

FIG. 9. Poincaré section for the values defined in Fig. 8. We have regular motion.

model a rotating star or the core of a galaxy. The black hole rotation produces the pure relativistic effect of dragging of inertial frames. Then our main goal in this section is to study the influence of the black hole rotation on the stability of geodesic motions. Letelier and Vieira [19] studied the motion of test particles moving around a slowly rotating black hole with a dipolar halo. Now we shall study the case of a central body with arbitrary rotation deformed by an internal quadrupole term.

The metric for a stationary axially symmetric space time has the general form

$$ds^2=g_{tt}dt^2+2g_{t\phi}dtd\phi+g_{\phi\phi}d\phi^2-e^{\Gamma}(u^2-v^2)\times\left[\frac{du^2}{u^2-1}+\frac{dv^2}{1-v^2}\right], \tag{15}$$

where g_{tt}, $g_{t\phi}$, $g_{\phi\phi}$, and Γ are function of the coordinates u,v.

To construct the solution of the vacuum Einstein that represents the superposition of a Kerr black hole and a field of multipoles, we use the Belinsky-Zakharov method [25]. In this method the Kerr space time is obtained from the Minkowski vacuum (seed solution) as a two-soliton solution. The application of this solution generating algorithm to more general seeds was studied by Letelier [32]. Some other recursive methods are described in Ref. [26]. Using the techniques presented in Ref. [32], we easily obtain the metric functions $g_{tt}(u,v)$, $g_{t\phi}(u,v)$, $g_{\phi\phi}(u,v)$, and $f(u,v)$ that represent a Kerr black hole deformed by multipolar terms. We choose a quadrupolar field as a seed solution. Then the Belinsky-Zakharov two-soliton transformation give us the nonlinear superposition of a Kerr solution with this field. We find

$$g_{tt}=[e^{H}(e^{2H}\{[2e^{2F_1+2F_2}(u^2-v^2)-e^{2H}(v^2-1)](p+1)^2-e^{4F_1}(u+1)(u-1)q^2\}q^2-e^{4F_2}[e^{2H}(p+1)^2(u+1)(u-1)+e^{4F_1}(v^2-1)q^2](p+1)^2)]/(e^{2H}\{[2e^{2F_1+2F_2}(u+v)(u-v)-e^{2H}(v-1)^2](p+1)^2e^{4F_1}(u-1)^2q^2\}q^2-e^{4F_2}\times[e^{2H}(p+1)^2(u+1)^2+e^{4F_1}(v+1)^2q^2](p+1)^2), \tag{16}$$

$$g_{t\phi}=\{-2e^{H}[e^{2H}\{[2e^{2F_1+2F_2}(u^2-v^2)-e^{2H}(v^2-1)](p+1)^2-e^{4F_1}(u+1)(u-1)q^2\}q^2-e^{4F_2}[e^{2H}(p+1)^2(u+1)(u-1)+e^{4F_1}(v^2-1)q^2](p+1)^2+(e^{2F_1}[e^{4F_2}(p+1)^2(u+1)(v+1)+e^{2H}(u-1)(v-1)q^2](u-v)-e^{2F_2}[e^{2H}(p+1)^2(u+1)\times(v-1)+e^{4F_1}(u-1)(v+1)q^2](u+v))(p+1)p]q\}/(e^{2H}\{[2e^{2F_1+2F_2}(u^2-v^2)-e^{2H}(v-1)^2](p+1)^2-e^{4F_1}(u-1)^2q^2\}q^2-e^{4F_2}[e^{2H}(p+1)^2(u+1)^2+e^{4F_1}(v+1)^2q^2](p+1)^2), \tag{17}$$

$$g_{\phi\phi}=\frac{g_{t\phi}^2-p^2(1-v^2)(u^2-1)}{g_{tt}}, \tag{18}$$

$$e^{\Gamma}=-(\exp[\{([(4[2\ln(u+1)+81u^2v^4-90u^2v^2+9u^2-36v^4+48v^2-8\ln(u+v)+14\ln(u-1)-8\ln(u-v)]+9(9u^2v^2-u^2-v^2+1)(u^2-1)(v^2-1)\ln[(u+1)/(u-1)]^2-12[27u^3v^4-30u^3v^2+3u^3-2-(21v^2-5)\times(v^2-1)u]\ln[(u+1)/(u-1)]\}k_2-16\{(3u^2-1)\ln[(u+1)/(u-1)]-6u\}(3v^2-1))k_2]/128)]\times(e^{2H}\{[2e^{2F_1+2F_2}(u^2-v^2)-e^{2H}(v-1)^2](p+1)+e^{4F_1}(p-1)(u-1)^2\}(p-1)+e^{4F_2}[e^{2H}(p+1)(u+1)^2-e^{4F_1}(p-1)(v+1)^2)(p+1)])/[4e^{2F_1+2F_2+2H}(u^2-v^2)p^2], \tag{19}$$

where

$$F_1=[-(2\{2[\ln(u+1)-3v^2-3\ln(u-1)+2\ln(u-v)]+3(3v-1)(v+1)u\}+3\{[v+3+2(v+1)u](v-1)-(3v-1)(v+1)u^2\}\ln[(u+1)/(u-1)])k_2]/16, \quad (20)$$

$$F_2=[-(2\{3[(3v-1)(v+1)u+2v^2]-4\ln(u+v)+4\ln(u-1)\}-3[(3v-1)u-(v+1)](u+1)(v+1)\times\ln[(u+1)/(u-1)])k_2]/16, \quad (21)$$

$$H=(\{(3u^2-1)\ln[(u+1)/(u-1)]-6u\}(3v^2-1)k_2)/8k_2/8. \quad (22)$$

The quadrupole strength is k_2, q is the source angular momentum per square of the mass, and p is defined by the relation $p^2+q^2=1$. The metric presented above is a particular case of the general solution that represents a Kerr metric embedded in a field of multipoles, see for instance Refs. [33] and [30].

When one performs the limit $k_2\to 0$ in the solution presented above, one obtains the Kerr metric in Boyer-Lindquist coordinates, r and ϑ that are related to the prolate spheroidal coordinates, u and v by $u=(r-m)/\sigma$, and $v=\cos\theta$. The constants p and q are related to the Boyer-Lindquist constants by $p=\sigma/m$, $q=a/m$, and $m^2=\sigma^2+a^2$, where m is the monopole mass, σ is an auxiliary constant, and a is interpreted as the black hole angular momentum per unit of mass measured by a very distant observer.

As in the preceding case, the geodesic equations have two constants of motion, L and E,

$$E=g_{tt}\dot{t}+g_{t\phi}\dot{\phi},$$

$$g_{\phi\phi}\dot{\phi}+g_{t\phi}\dot{t}=L. \quad (23)$$

The evolution equations for u and v are

$$\frac{d^2u}{d\tau^2}=\frac{u^2-1}{2\Gamma(u^2-v^2)}[\partial_u g_{tt}\dot{t}^2+2\partial_u g_{t\phi}\dot{t}\dot{\phi}+\partial_u g_{\phi\phi}\dot{\phi}^2]-\dot{u}^2\left[\frac{\partial_u\Gamma}{2\Gamma}+\frac{(v^2-1)u}{(u^2-v^2)(u^2-1)}\right]-2\dot{u}\dot{v}\left[\frac{\partial_v\Gamma}{2\Gamma}-\frac{v}{(u^2-v^2)}\right]-\dot{v}^2\left[\frac{\partial_u\Gamma(u^2-1)}{2\Gamma(v^2-1)}+\frac{(u^2-1)u}{(u^2-v^2)(v^2-1)}\right], \quad (24)$$

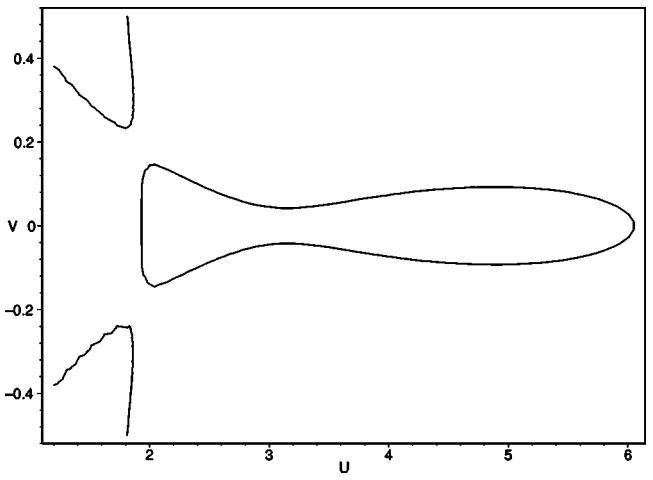

FIG. 10. Boundary contour of the Kerr-quadrupole system for $L=-3.322$, $E=0.937\,15$, $k_2=-5.08$, and $q=0.002$.

$$\frac{d^2v}{d\tau^2}=\frac{1-v^2}{2\Gamma(u^2-v^2)}[\partial_v g_{tt}\dot{t}^2+2\partial_v g_{t\phi}\dot{t}\dot{\phi}+\partial_v g_{\phi\phi}\dot{\phi}^2]-\dot{v}^2\left[\frac{\partial_v\Gamma}{2\Gamma}-\frac{(u^2-1)v}{(u^2-v^2)(v^2-1)}\right]-2\dot{u}\dot{v}\left[\frac{\partial_u\Gamma}{2\Gamma}+\frac{u}{(u^2-v^2)}\right]-\dot{u}^2\left[\frac{\partial_v\Gamma(v^2-1)}{2\Gamma(u^2-1)}-\frac{(v^2-1)v}{(u^2-v^2)(u^2-1)}\right]. \quad (25)$$

Also, as before we have two second-order evolution equations (24) and (25) for the variables u and v, the metric and the constants (23) give a new constant relating these two variables,

$$1=g^{tt}E^2+2g^{t\phi}EL+g^{\phi\phi}E^2-e^{\Gamma}(u^2-v^2)\times\left[\frac{\dot{u}^2}{u^2-1}+\frac{\dot{v}^2}{1-v^2}\right]. \quad (26)$$

In other words, despite algebraic complications, we have exactly the same dynamical situation as in the static case. The particles move in an effective three-dimensional space. Thus we can analyze the motion of test particles moving in the gravitational field of a rotating prolate deformed body using Poincaré sections as in the nonrotating case.

Since the main new ingredient in the system under consideration is the rotation of the source, we shall keep the angular momentum L, the energy E, and the quadrupole strength k_2 fixed; and we shall consider test particles moving with angular momentum parallel to the spin source (corotation) and with angular momentum counterparallel to the spin source (counter-rotation).

In Fig. 10 we present the region of bounded motions for counter-rotating orbits, $qL<0$. We take $E=0.937\,15$, $|L|=3.322$, and $k_2=-5.08$, and for the rotation parameter $q=0.002$. We have a situation similar to the one presented in Fig. 2. The bounded regions for the corotation case, qL

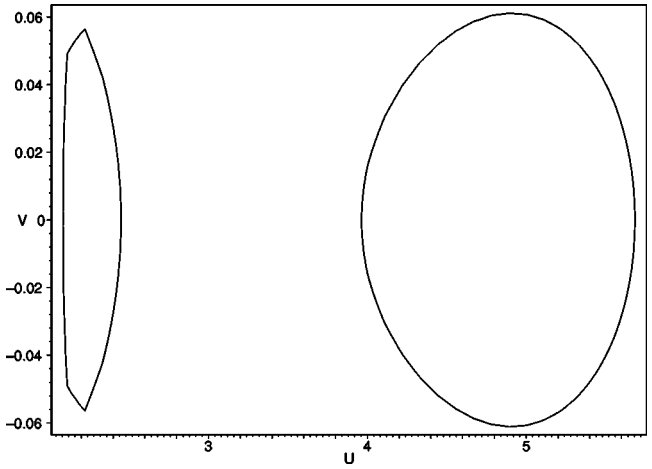

FIG. 11. Boundary contour for a Kerr-quadrupole system for $L=3.322$, $E=0.937\,15$, $k_2=-5.08$, and $q=0.002$. The confinement region is separated in two, they are much smaller than in the preceding figure.

>0, is shown in Fig. 11. We see two relatively small and distant closed surfaces. The Poincaré section for the counter-rotating case is presented in Fig. 12. Chaotic motion can be seen on the left of the graphic and in the external part of the right-hand side, as in Fig. 6. In Fig. 13, we present the surface section for the same parameters as above, but $qL>0$ (corotation). We do not find chaotic motion in this case.

We were not able to obtain bounded motion for both large quadrupole strengths and large rotation parameters. We study bounded systems with large rotation speed (of the order of 0.1), but with quadrupole strength always less than unity. In these cases, the study of Poincaré sections leads to regular geodesic motion for corotation as well as counter-rotation. We also found that the confinement region may suffer an appreciable change in size and shape.

DISCUSSION

Besides the results presented in the previous sections we have constructed some Poincaré surfaces for the external dipole plus black hole solution. We also study combinations including internal octopole and external quadrupole terms, rotating sources were considered as well. We found that for the great majority of values of momentum and energy, which confined the motion there are only regular orbits, in general, chaotic geodesics are found near the central mass for distances less than 50 black hole masses (in geometric units). Therefore, we conclude that observational consequences of the geodesic instabilities will be mostly relevant in a very restricted area close to the black hole.

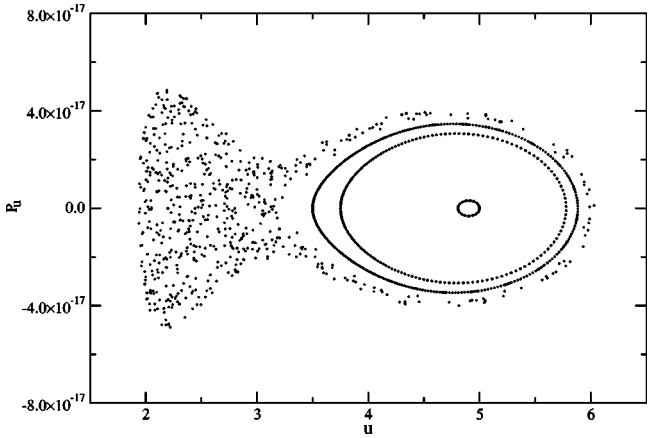

FIG. 12. Poincaré section for the same value of the parameters of Fig. 10. We have chaotic motion mainly in the left-hand side of the picture.

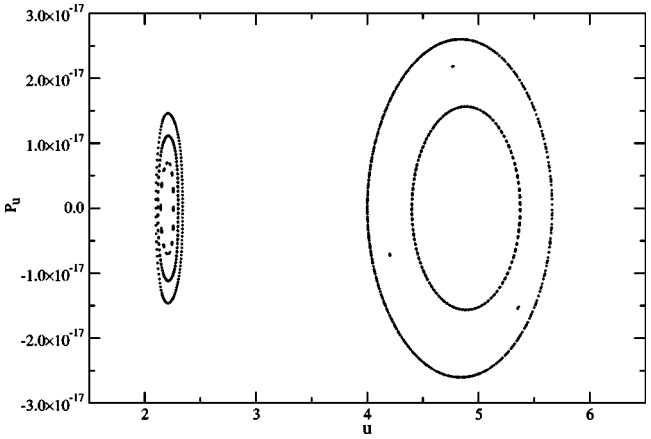

FIG. 13. Poincaré section for the same value of the parameters of Fig. 11. We do not see irregular motion in both regions.

Large rotations, $1>q\geqslant 0.1$, were analyzed studying some Poincaré sections for a solution that represents a monopole surrounded by a dipolar halo. We did not find an internal quadrupole solution with large rotation and quadrupole strength of the same order of the static examples studied in the preceding sections because the bounded regions completely disappear for large rotations. We present three Poincaré sections for a rotating black hole plus dipole solution using the parameters $L=3.988$, $E=0.9665$, and $D=0.0005$. In Fig. 14 we consider a static black hole. In Fig. 15, a rotating system is considered with rotation parameter $q=5/13$, the geodesics corresponding to the corotating or-

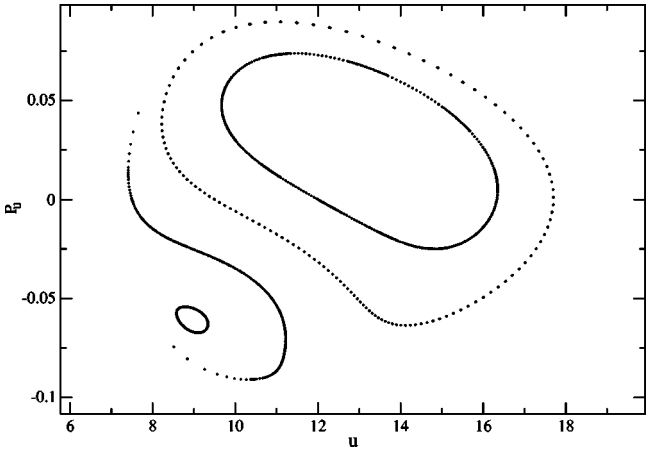

FIG. 14. Poincaré section for the static black hole plus dipole solution using $L=3.988$, $E=0.9665$, and $D=0.0005$. It looks like an integrable motion.

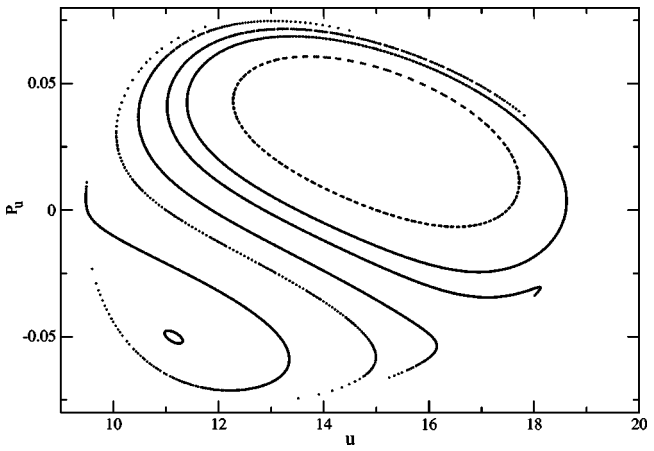

FIG. 15. The same as the preceding figure, but now we add rotation, $a/m=5/13$. The center of attraction is a rotating black hole with a dipolar halo.

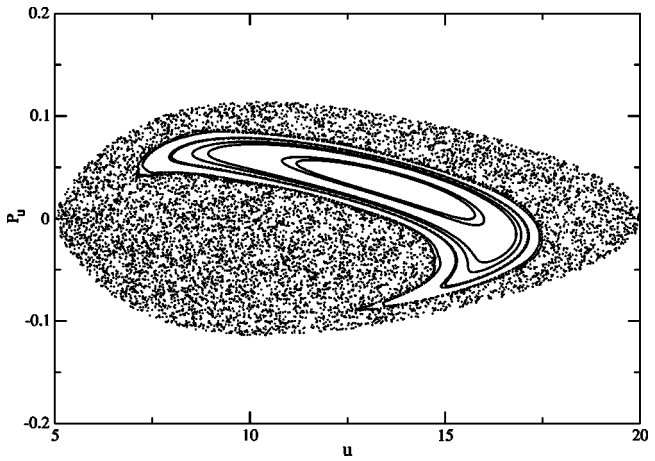

FIG. 16. A surface of section with the same parameters of Fig. 15, but for counterrotating orbits ($Lq<0$). Irregular motion is seen here.

bits. In both figures there are apparently only nonchaotic orbits in phase space. This situation changes completely for counter-rotation, using the same parameters of Fig. 15, but $q=-5/13$, we find in Fig. 16 the surface of section of chaotic orbits.

The main results of this paper are: We find chaotic geodesics in the geometry that characterizes an internal quadrupole plus monopole solution for the prolate case. In the oblate case these orbits appear to be regular. This behavior is similar to the Newtonian analogs, except for the fact that the closed region that confines the chaotic orbits are very different [33–35].

For rotating sources we see that large speeds alter significantly the bounded regions, and consequently chaotic regions for counter-rotation arise in situations where the static case seems to be nonchaotic. We conclude that observational effects may be found for this group of orbits. In spite of these modifications, it is also very difficult (perhaps impossible) to find chaotic geodesics around rotating sources with an oblate quadrupolar deformation, like that in the static case. This result tells us that there are no numerical evidences of the existences of nonintegrable geodesics in the internal quadrupole plus monopole solution in general relativity. In other words it does look like that the motion of test particles orbiting around internal an oblate quadrupole plus monopole center of attraction in the Newtonian gravitation, as well as, in the general relativity are integrable. To prove the integrability of these systems is not an easy task. Also to perform a Painlevé type of analysis [36] for these cases is quite involved,

This work intends to complete the study of chaos of geodesic motion in axially symmetric metrics obtained from a multipolar expansion. We think that the next natural step is the study of stability of astrophysical structures confined in situations described by this model, specially when general relativistic effects can make a difference.

The exact solution to Einstein equations presented in the preceding sections are not new, and different versions of them have already appeared in the literature. We present them in this work for two reasons: (a) for easy reference, and (b) mainly, because for numerical analysis we need a faultless solution. The ones presented here were derived using algebraic computation and checked using the full vacuum Einstein equations in each case.

ACKNOWLEDGMENTS

The authors thank FAPESP for financial support. P.S.L. also thanks CNPq.

[1] H. Poincaré, *Les Méthodes Nouvelles de la Mechanique Celeste* (Gauthier-Villars, Paris, 1892).

[2] A. N. Kolmogorov, Dokl. Akad. Nauk SSSR **98**, 527 (1954); V. I. Arnol'd., Russ. Math. Survey **18**, 9 (1963); **18**, 85 (1963); J. Moser, Math. Appl. **169**, 136 (1967).

[3] M. V. Berry, in *Topics in Nonlinear Dynamics A Tribute to Sir Edward Bullard*, edited by Siebe Jorna, AIP Conf. Proc. No. 46 (AIP, New York, 1978), p. 16.

[4] D. Merrit, Science **271**, 337 (1996).

[5] See, for instance, H. Robertson and T. Noonan, *Relativity and Cosmology* (Saunders, London, 1968), pp. 272–278.

[6] See, for instance, C. M. Cosgrove, J. Math. Phys. **23**, 615 (1982), and references therein.

[7] G. Contopoulos, Proc. R. Soc. London, Ser. A **431**, 183 (1990); **435**, 551 (1991).

[8] Y. Sota, S. Suzuki, and K. Maeda, Class. Quantum Grav. **13**, 1241 (1996); see also, W. M. Vieira and P. S. Letelier, *ibid.* **13**, 3115 (1996).

[9] W. M. Vieira and P. S. Letelier, Phys. Lett. A **288**, 22 (1997).

[10] L. Bombelli and E. Calzetta, Class. Quantum Grav. **9**, 2573 (1992).

[11] P. S. Letelier and W. M. Vieira, Class. Quantum Grav. **14**, 1249 (1997).

[12] S. Chandrasekhar, *The Mathematical Theory of Black Holes* (Clarendon Press, Oxford, 1983).
[13] See, for instance, Ya. B. Zeldovich and I. D. Novikov, *Relativistic Astrophysics* (University of Chicago Press, Chicago, 1971), pp. 130–134; M. Carmeli, *Classical Fields: General Relativity and Gauge Theory* (Wiley, New York, 1982), pp. 177–182.
[14] F. Bertola *et al.*, Astrophys. J. **458**, L67 (1996).
[15] A. R. Cooray, Mon. Not. R. Astron. Soc. **313**, 783 (2000).
[16] B. Carter, Phys. Rev. Lett. **26**, 331 (1971).
[17] W. M. Vieira and P. S. Letelier, Astrophys. J. **513**, 383 (1999); Phys. Rev. Lett. **76**, 1409 (1996).
[18] A. P. S. Moura and P. S. Letelier, Phys. Rev. E **61**, 6506 (2000).
[19] P. S. Letelier and W. M. Vieira, Phys. Rev. D **56**, 8098 (1997).
[20] A. Saa and R. Venegeroles, Phys. Lett. A **259**, 201 (1999); see also, A. Saa, *ibid.* **269**, 204 (1999).
[21] P. S. Letelier and W. M. Vieira, Phys. Lett. A **244**, 324 (1998).
[22] A. P. S. Moura and P. S. Letelier, Phys. Lett. A **266**, 309 (2000); P. S. Letelier and W. M. Vieira, *ibid.* **242**, 7 (1998); P. S. Letelier and A. E. Motter, Phys. Rev. E **60**, 3920 (1999).
[23] E. Guéron and P. S. Letelier, Astron. Astrophys. **368**, 716 (2001); H. Varvoglis and D. Papadopoulos, *ibid.* **261**, 664 (1992); V. Karas and D. Vokrouhlicky, Gen. Relativ. Gravit. **24**, 729 (1992).
[24] E. Guéron and P. S. Letelier, Phys. Rev. E **63**, 035201(R) (2001).
[25] V. A. Belinsky and V. Zakharov, Sov. Phys. JETP **50**, 1 (1979).
[26] D. Kramer, H. Stephani, and E. Herlt, *Exact Solution of Einstein's Field Equations* (Cambridge University Press, Cambridge, England, 1980).
[27] J. Ehlers, in *Grundlagenprobleme der Modernen Physik*, edited by A. Erdélyi, J. Pfarr, and E.-W. Stachov (Verlag, Mannheim, 1981), pp. 65–84.
[28] G. Erez and N. Rosen, Bull. Res. Counc. Isr., Sect. F **8**, 47 (1959).
[29] H. Quevedo, Phys. Rev. D **39**, 2904 (1989).
[30] P. S. Letelier, Class. Quantum Grav. **16**, 1207 (1999).
[31] B. Boisseau and P. S. Letelier, Gen. Relativ. Gravit. **34**, 1077 (2002).
[32] P. S. Letelier, J. Math. Phys. **26**, 467 (1984).
[33] H. Quevedo and B. Mashhoon, Phys. Rev. D **43**, 3902 (1991).
[34] J. Levin, Phys. Rev. D **60**, 4015 (1999).
[35] J. Binney and S. Tremaine, *Galactic Dynamics* (Princeton University Press, New Jersey, 1987).
[36] See, for instance, M. Tabor, *Chaos and Integrability in Nonlinear Dynamics* (Wiley, New York 1989).